

Latitude-Dependent Time Variations of the Solar Tachocline

SARBANI BASU ¹, SYLVAIN G. KORZENNIK ² AND SUSHANTA C. TRIPATHY ³

¹*Department of Astronomy, Yale University, PO Box 208101, New Haven, CT 06520-8101, USA*

²*Center for Astrophysics | Harvard & Smithsonian, Cambridge, MA 02138, USA*

³*National Solar Observatory, 3665 Discovery Dr., Boulder, CO 80303, USA*

ABSTRACT

We have examined how the characteristics of the tachocline — i.e., the change in rotation rate $\delta\Omega$, or the “jump”, the position of the midpoint of the tachocline, r_d , and the width of the tachocline, w_d , — change as a function of time at different latitudes using 30 years of helioseismic data obtained by the GONG network. We find a statistically significant change in the jump, however, these changes do not have a simple correlation with solar activity. The dependence is different for solar Cycles 23 and 24, and for Cycle 25, it is more similar to that of Cycle 24. While our measured changes of the tachocline’s width with time are marginally statistically significant, the cross correlation is statistically significant and implies that the width is larger when the solar activity is smaller, suggesting that magnetic fields play a role in confining the tachocline. The position of the tachocline shows a significant secular change at low latitudes ($\lesssim 50^\circ$). At these latitudes, the tachocline has been moving steadily closer to the base of the convection zone. This is consistent with other measurements that have shown that the overall complexity of solar activity has been decreasing over the last few decades. It leads us to speculate that strong magnetic fields tend to push the tachocline deeper into the radiative zone.

Keywords: The Sun (1693) — solar oscillations (1515) — helioseismology (709) — solar rotation (1524)

1. INTRODUCTION

Inversions of helioseismic data have shown that the convection zone (CZ) of the Sun rotates differentially, while the radiative interior rotates like a solid body (e.g., J. Schou et al. 1998, etc.). Connecting the two zones is a thin shear layer, known as the tachocline.

While neither the role nor the origin of the tachocline is well understood, a set of solar dynamo models depends on the strong shear in this region to convert weak poloidal fields into strong toroidal fields (e.g., M. Dikpati & P. Charbonneau 1999; P. Chatterjee et al. 2004; G. Guerrero & E. M. de Gouveia Dal Pino 2008, and references therein). If indeed the tachocline is the location of the solar dynamo where magnetic fields are generated, one would expect solar-cycle related changes in the properties of the tachocline.

S. Basu & H. M. Antia (2019) showed that the change in the rotation rate between the solar CZ and the radiative zone (the “jump”) is a function of time; however, the temporal dependence is not a simple correlation with

magnetic activity. The jump followed different trends during solar Cycle 23 than solar Cycle 24 and, furthermore, had different values at the same level of solar activity. S. Basu et al. (2024) found a similar result by analyzing only the most dominant component of the tachocline that showed a $\cos^2 \vartheta$ variation with the colatitude ϑ . They further speculated that there is a longer cycle — longer than either the 11-year solar cycle or the 22-year magnetic cycle — that modulates the tachocline jump.

S. Basu & H. M. Antia (2019) did not detect any changes in the position of the tachocline or the width of the tachocline because of the magnitude of the uncertainties caused by large error bars in the helioseismic data they used. These were splitting coefficients derived using the respective project reduction pipelines, namely from fitting 108-day time series of observations by the Global Oscillation Network Group (GONG: F. Hill et al. 1996) and 72-day time series of observations by the Michelson Doppler Imager (MDI: P. H. Scherrer et al. 1995), an instrument on board the Solar and Heliospheric Observatory (SOHO) and later from observations by the Helioseismic and Magnetic Imager (HMI: P. H. Scherrer et al. 2012), an instrument on board the

Solar Dynamics Observatory (SDO). Subsequent analysis using longer data sets (S. Basu et al. 2024) did find significant changes in the width and position of the tachocline; however, as mentioned earlier, that work only examined the most dominant splitting coefficients with respect to latitude, which is, of course, an incomplete characterization of the tachocline.

In this paper, we present results of a more complete, two-dimensional analysis of changes of the properties of the tachocline using approximately 2-year-long time series. S. Basu et al. (2024) found that although data sets obtained with longer time series (1152, 2304, and 4608 days) were more precise, they tended to wash out solar-cycle-related variations. We also use data sets derived from shorter time series for examining changes in the jump of the tachocline, since it is easier to determine that property precisely.

The remainder of this paper is organized as follows. We describe our tachocline model, the fitting method, and data used in Section 2. We describe our results in Section 3, and discuss and summarize our findings in Section 4.

2. THE TACHOCLINE MODEL AND DATA USED

At all latitudes, we model the tachocline as a sigmoid following S. Basu (1997), H. M. Antia et al. (1998), and S. Basu et al. (2024):

$$\Omega(r)_{\text{tach}} = \frac{\delta\Omega}{1 + \exp[-(r_d - r)/w_d]}, \quad (1)$$

where $\delta\Omega$ is the jump in the rotation rate between the convection zone and the interior, r_d is the position of the tachocline, defined as the midpoint of the transition (or discontinuity), and w_d is the width of the transition layer. In this model, the rotation rate changes from $0.269\delta\Omega$ to $0.731\delta\Omega$ between $r = r_d - w_d$ and $r = r_d + w_d$. Note that the sign of $\delta\Omega$ tells us whether the convection-zone rotation rate is higher than the radiative-zone rate or vice versa. The magnitude, $|\delta\Omega|$, tell us how large the jump is.

Note that there is another model of the tachocline, that of A. G. Kosovichev (1996), that has been used in the literature, where the model uses an error function as follows:

$$\Omega_{\text{tach,Erf}}(r) = \frac{\delta\Omega}{2} \left\{ 1 + \operatorname{erf} \left[2 \frac{(r - r_d^{(e)})}{w_d^{(e)}} \right] \right\}, \quad (2)$$

where $\delta\Omega$ is the change in the rotation rate across the tachocline and $r_d^{(e)}$ is the midpoint of the tachocline. For this model, $w_d^{(e)}$ is the radial extent over which the model varies from 0.08 to 0.92 of $\delta\Omega$. Using this model

does not change the results for the position, while the width, $w_d^{(e)}$, however, is different, and for small widths (as we find in this work, see § 3.2), $w_d^{(e)}$ is five times w_d ; S. Basu (1997) showed that the two definitions give similar results for the other tachocline parameters.

Since we are investigating latitude-dependent changes, the quantities $\delta\Omega$, r_d and w_d are modeled as functions of colatitude, ϑ , as follows:

$$\delta\Omega = \delta\Omega_3 P_3(\vartheta) + \delta\Omega_5 P_5(\vartheta), \quad (3)$$

$$r_d = r_{d1} + r_{d3} P_3(\vartheta), \quad (4)$$

and

$$w_d = w_{d1} + w_{d3} P_3(\vartheta), \quad (5)$$

where the functions P_3 and P_5 are defined as:

$$\begin{aligned} P_3(\vartheta) &= 5 \cos^2 \vartheta - 1, \\ P_5(\vartheta) &= 21 \cos^4 \vartheta - 14 \cos^2 \vartheta + 1. \end{aligned} \quad (6)$$

This latitudinal variation is quite similar to that used by P. Charbonneau et al. (1999), who used a simple $\cos^2 \vartheta$ variation, with $r_d(\vartheta) = r_{d,0} + r_{d,1} \cos^2 \vartheta$ and $w_d(\vartheta) = w_{d,0} + w_{d,1} \cos^2 \vartheta$. We prefer to keep our dependence explicitly in terms of $P_3(\vartheta)$ since that is the angular dependence of the splitting coefficients used, and hence a more fundamental assumption; this also allowed us to test the effect of higher-order coefficients in a previous work (S. Basu & S. G. Korzennik 2025). Changing the latitudinal dependence from that in Eq. 4 to that of P. Charbonneau et al. (1999) does not change the results.

The complete model is the same as that used by S. Basu & H. M. Antia (2019):

$$\Omega(r, \vartheta) = \begin{cases} \Omega_c + \Omega_{\text{tach}} & \text{if } r \leq 0.7R_\odot \\ \Omega_c + B(r - 0.7) + \Omega_{\text{tach}} & \text{if } 0.7 < r \leq 0.95R_\odot \\ \Omega_c + 0.25B - C(r - 0.95) + \Omega_{\text{tach}} & \text{if } r > 0.95R_\odot, \end{cases} \quad (7)$$

where Ω_c , B and C are free parameters, and $\delta\Omega_{\text{tach}}$ is given by Eq. 1.

We determine the tachocline parameters using simulated annealing (D. Vanderbilt & S. G. Louie 1984; W. H. Press et al. 1992) to minimize a least-squares fit between the observed and computed values of the data. This algorithm uses randomly generated initial values of the model parameters, and we assume that these parameters have Gaussian priors with their mean and width determined from existing inversions of rotational splittings. Since there is a finite chance that the solution

becomes trapped in a local minimum, we make 100 different realizations using different sequences of randomly selected initial guesses in order to determine a global χ^2 minimum. We confirm whether the algorithm reached a global minimum by inspecting the likelihood-weighted distribution of all the parameters for all iterations. This distribution is single-peaked when a global χ^2 minimum is reached; otherwise, it will have multiple peaks (or be flat if the parameter cannot be constrained). We determine uncertainties of the model parameters using the traditional bootstrapping method of simulating many realizations of the observations and fitting each one of them in the same manner as the original data, and we use the spread as a measure of uncertainty (P. J. M. Laarhoven & E. H. L. Aarts 1987). Note that the lower error bars that result from fitting longer time series allow one to fit additional terms in the expansion of r_d with respect to the colatitude (as shown by S. Basu & S. G. Korzennik 2025); however, the 720-day sets do not allow us to do so.

The data used in this work are derived from ground-based solar oscillation observations acquired by the GONG instruments. GONG has been observing the Sun without interruption since 1995; hence, these data are ideal for studying time variations of the solar interior.

Most of the rotational frequency splittings that we use were obtained by an independent data reduction pipeline, which we refer to as the ‘‘SGK’’ pipeline (S. G. Korzennik 2004, 2008a,b; S. G. Korzennik & A. Eff-Darwich 2013; S. G. Korzennik 2017, 2018, 2023) after the author of the pipeline. The SGK pipeline derives mode parameters from time series that are multiples of 72 days. For this work, we use splittings obtained with 144-day time series and 720-day time series, with the 720-day data sets having a 360-day overlap. While the GONG project does not routinely produce frequencies with 144-day or 720-day time series, a custom 720-day non-overlapping set of frequencies and splittings was produced for this work by co-author SCT using the GONG project pipeline. As mentioned earlier, the data obtained with the shorter time series are used to determine the jump, while the longer time series data are used to determine the other parameters.

The sets are available in the standard form, i.e., expressed as follows:

$$\nu_{nlm} = \nu_{nl} + \sum_{j=1}^{j_{\max}} c_j(n, l) \mathcal{P}_j^{(l)}(m), \quad (8)$$

where ν_{nl} , the central frequency of a mode of degree l and radial order n , is determined by the spherically symmetric part of the solar structure, c_j are splitting coefficients, and \mathcal{P}_j are rescaled Clebsch-Gordon coef-

ficients (see M. H. Ritzwoller & E. M. Lively 1991). With the oscillation frequencies expressed in this form, one can show that the odd-order c_j are caused by the solar rotation and have information about the latitudinal distribution, while the even-order coefficients contain signatures of asphericity and magnetic fields. We work with the c_j coefficients as defined by M. H. Ritzwoller & E. M. Lively (1991); both the SGK and the GONG project pipelines, produce these.

As with S. Basu & S. G. Korzennik (2025), we restrict ourselves to using modes with frequencies between 1.5 mHz and 3.5 mHz that have lower turning points between $0.55R_\odot$ and $0.85R_\odot$ for the range of degrees that is covered by the data set. Note that the lower turning point is the deepest location a mode penetrates, according to ray theory, and effectively the depth below which the oscillation sensitivity decreases drastically; mode properties are most affected by the structure and dynamics at that depth. This subset gives good coverage of the tachocline, while keeping the uncertainties low (modes with lower and higher frequencies have larger uncertainties). This choice of modes also removes the need to properly account for the near-surface shear layer in the tachocline model, although, as Eq. 7 shows, we do model that layer, albeit crudely. We opted to use the 10.7 cm radio flux as a measure of solar activity (K. F. Tapping 2013; K. F. Tapping & D. C. Morton 2013).

3. RESULTS

3.1. The jump, $\delta\Omega$, across the tachocline

We show the two components of the jump in rotation rate across the tachocline, $\delta\Omega_3$ and $\delta\Omega_5$, as a function of time in Fig. 1. Note how their variations with time measured with either the 144-day or the 720-day sets agree with each other. Variations measured using data sets resulting from the SGK and the GONG project pipelines show the same time dependence, though there are small differences in the magnitude of the jump. In general, the GONG project pipeline’s data sets produce slightly higher values of $\delta\Omega_5$ at the rising phases of activity and slightly smaller values at declining phases; the differences in estimates of $\delta\Omega_3$ are more random, though.

What should be noted is that the component Ω_3 , which is essentially determined by the splitting coefficient c_3 , does not have a simple solar-cycle dependence. This is in line with what was found by S. Basu et al. (2024), which is not surprising, given that they had used c_3 in that work, and also that the rotational frequency splittings are expanded using orthogonal polynomials.

One can see that the jump, given by the absolute value of the $\delta\Omega_3$ component, started increasing in the falling phase of Cycle 23, had a somewhat flat time dependence

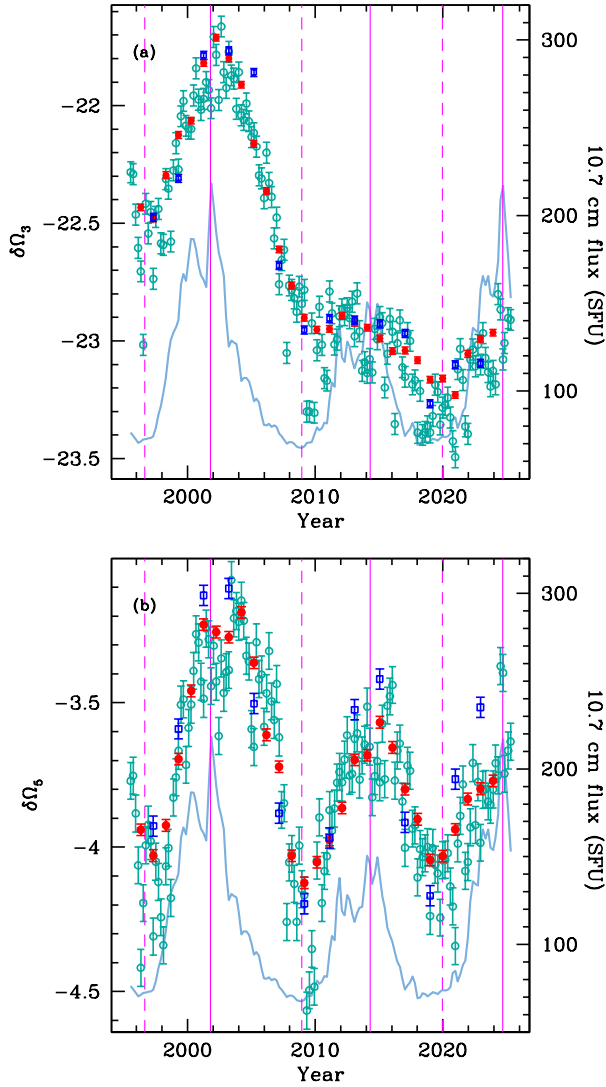


Figure 1. The $\delta\Omega_3$ and $\delta\Omega_5$ components of the change in the rotation rate across the tachocline plotted as a function of time, in panels labeled (a) and (b), respectively. The greenish-blue points are results for 144-day data sets using the SGK pipeline, the red points are results for 720-day data sets also using the SGK pipeline, while the blue points correspond to results for 720-day data sets using the GONG project pipeline. Values are plotted at the midpoint of the respective time series. The light blue line shows the 10.7 cm radio flux averaged over the 144 days corresponding to each data set. The radio flux magnitude can be read from the axes on the right-hand side of the panels. The solid and dashed vertical lines are epochs of solar maxima and minima, respectively.

during the rising phase of Cycle 24, increased again in the falling phase of that cycle, and started decreasing in the rising phase of Cycle 25. The second component of the jump, i.e., $\delta\Omega_5$, on the other hand, rises and falls with solar activity. The two, however, do not change

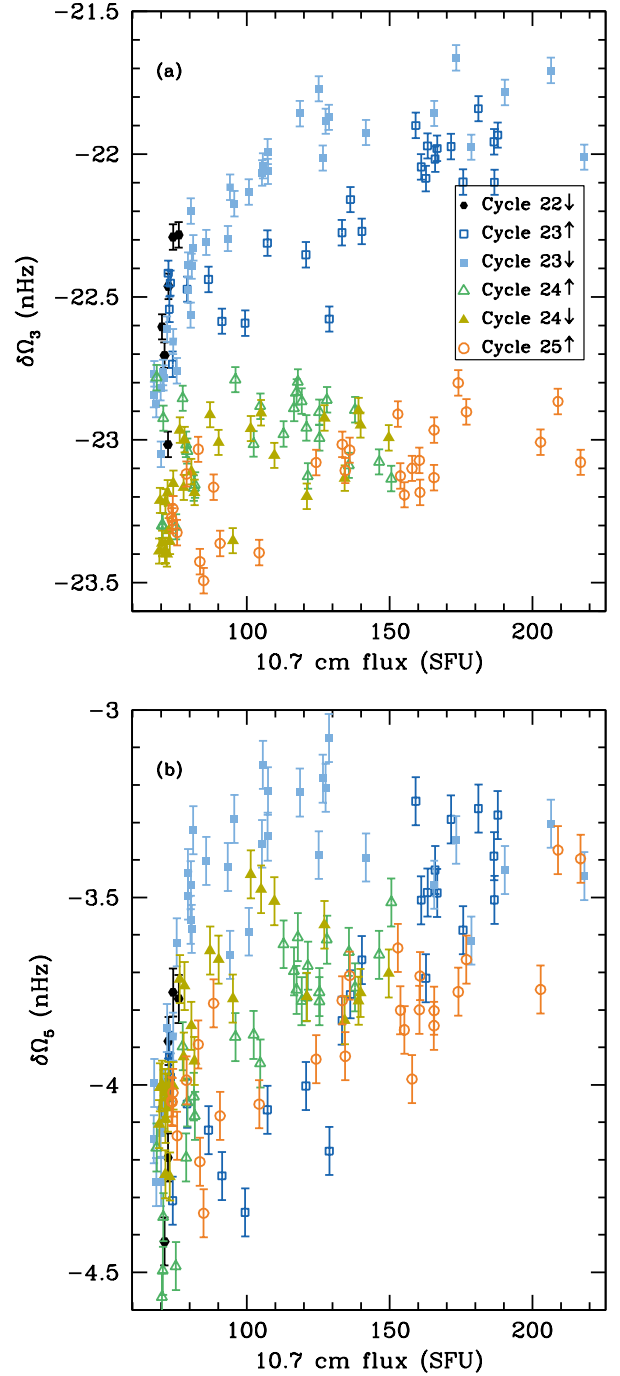


Figure 2. The $\delta\Omega_3$ and $\delta\Omega_5$ components of the change in the rotation rate across the tachocline plotted as a function of the 10.7 cm radio flux in panels labeled (a) and (b), respectively. Only results using the 144-day data sets are shown. The points are color-coded by the phase of the solar cycle, as described by the legend in panel (a), where the upward and downward arrows correspond respectively to the ascending and descending phases of the cycle.

in lockstep, and there is a time lag, as well as cycle-to-cycle differences. For instance, $\delta\Omega_5$ kept decreasing well after the minimum between Cycles 22 and 23, even after Cycle 23 had started rising, while the minimum in $\delta\Omega_5$ between solar Cycles 23 and 24 occurred at the activity minimum, as it did for the Cycle 24–25 minimum.

Table 1. The slope and p -values obtained for a linear regression of $\delta\Omega$ with respect to the 10.7 cm radio flux. The slope is in units of nHz (SFU) $^{-1}$.

Cycle & Phase	$\delta\Omega_3$		$\delta\Omega_5$	
	Slope	p-value	Slope	p-value
Cycle 23				
Ascending	5.62E-3	< 1E-4	7.31E-3	< 1E-4
Descending	7.33E-3	< 1E-4	3.99E-3	< 1E-4
Cycle 24				
Ascending	1.12E-3	2.24E-1	1.00E-2	< 1.3E-3
Descending	4.12E-3	6.48E-4	5.16E-3	< 7.0E-4
Cycle 25				
Ascending	2.64E-3	< 1E-4	3.90E-3	< 1E-4

Both components of the jump show a hysteresis-like behavior with respect to solar activity, as shown in Fig. 2. There are two notable points that we can draw from that figure: first, Cycles 23 and 24 do not show the same pattern of variation with solar activity levels. This is very clear for $\delta\Omega_3$, and is also present, though not as clearly, for $\delta\Omega_5$. Secondly, the pattern for Cycle 25 is similar to that of Cycle 24, even though it is as strong as Cycle 23. This leads us to speculate again (see S. Basu et al. 2024) that the jump across the tachocline during Cycle 26 is likely to follow the pattern we see for Cycle 23. In other words, there might be a four-solar-cycle periodicity in the jump across the tachocline. Obviously, confirming this hypothesis will require about 10 additional years of observations.

We have performed a linear regression analysis of $\delta\Omega_3$ and $\delta\Omega_5$ with respect to the 10.7 cm radio flux, and the results are tabulated in Table 1. The lack of correlation of $\delta\Omega_3$ during the rising phase of Cycle 24 is reflected in the corresponding p -value.

Although the latitudinal dependence of the jump in the tachocline and changes thereof is implicit in Figs. 1 and 2, we illustrate this dependence explicitly at five latitudes in Figs. 3 and 4. Fig. 3 shows a clear trend with solar activity only at 30° and 60° latitudes. At the latitude of 30° the magnitude of the jump decreases as solar activity decreases, while the opposite is true at the 60° latitude. Of course, we need to keep in mind that the transition as a function of latitude is quite gentle; the

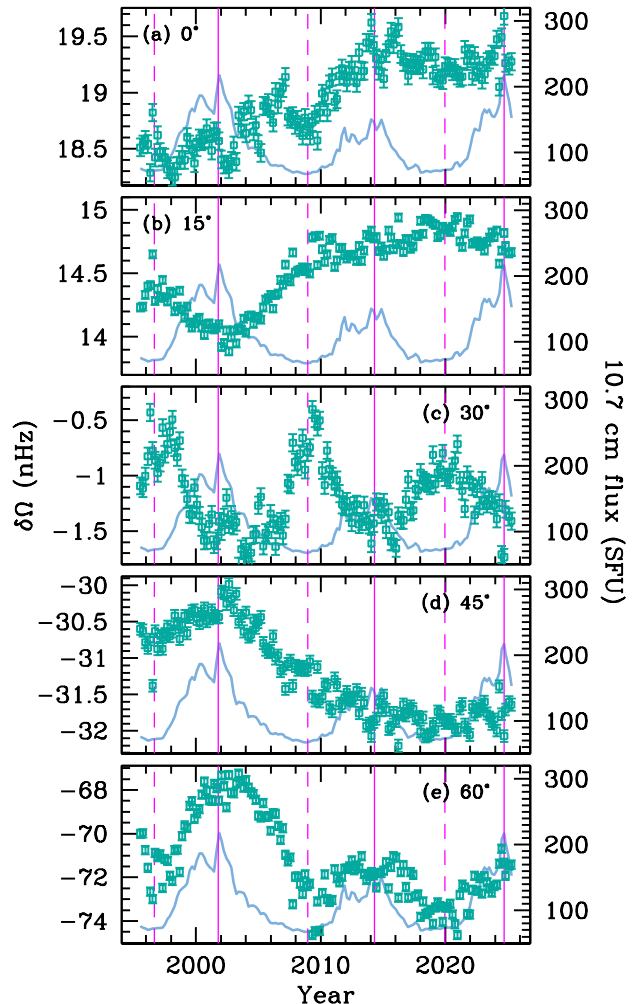


Figure 3. The change in the rotation rate across the tachocline at different latitudes plotted as a function of time. Panels (a)–(e) show the results at latitudes 0, 15, 30, 45, and 60°. Only 144-day results are shown. The light blue line shows the 10.7 cm radio flux averaged over 144 days; the magnitude of the radio flux can be read from the axes on the right-hand side of the panels. The solid and dashed vertical lines are epochs of solar maxima and minima, respectively.

stark change between panels (b), (c), and (d) is a result of only plotting the jump at a selected few latitudes. The jumps at different latitudes plotted as a function of activity (Fig. 4) show that at all latitudes the patterns followed by the jump during different solar cycles are different and that the patterns seen in Cycle 25 are similar to the ones seen in Cycle 24.

The jump around the latitude of 30° is interesting. Indeed, the conventional view, based on rotation inversions, is that the jump across the tachocline becomes zero at 30°. Such inversions, however, often do not have very good latitudinal resolution (see, e.g., J. Schou et al.

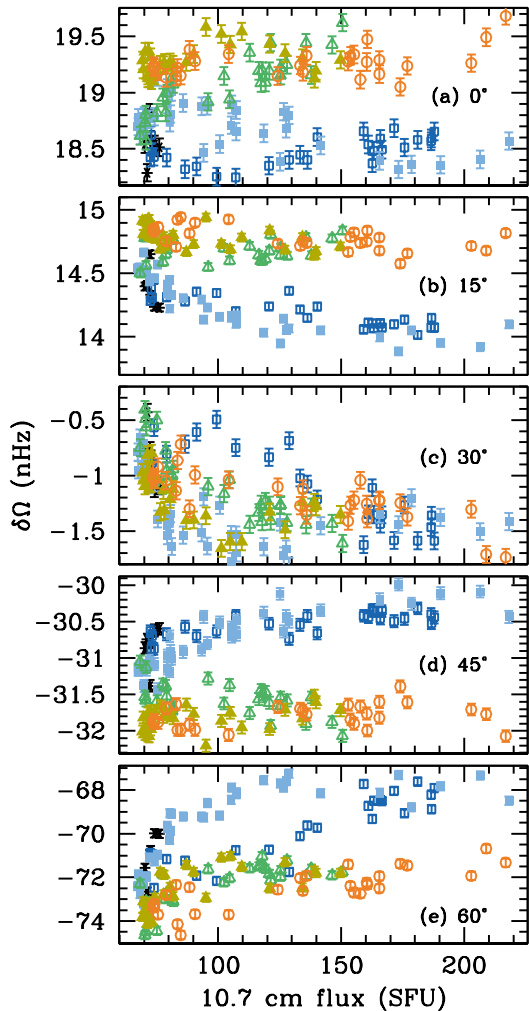


Figure 4. The change in the rotation rate across the tachocline at different latitudes plotted as a function of the 10.7 cm radio flux. Panels (a)–(e) show the results at latitudes 0, 15, 30, 45, and 60°. Only 144-day results are shown. The points are color-coded by the phase of the solar cycle using the same convention as in Fig. 2, i.e., black points for the descending phase of Cycle 22, dark blue empty squares for ascending Cycle 23, light blue filled squares for descending Cycle 23, dark green empty triangles for ascending Cycle 24, light green filled triangles for descending Cycle 24, and orange points for ascending Cycle 25.

1998), hence, the actual latitude at which $\delta\Omega$ vanishes, hereafter θ_v , is not very well determined. Our forward analysis technique allows us to determine θ_v , which we show in Fig. 5. This figure indicates that θ_v has a clear solar-cycle dependence; however, this change is not in lockstep with the solar activity cycle. New inversion results (S. G. Korzenik & A. Eff-Darwich 2026) indicate that the latitudinal resolution is around 8° even when much longer time series data are used; the resolution is

expected to be worse for the shorter sets that we are using. Thus, the resolution element in traditional inversions is much larger than the differences that we are seeing, explaining why this intriguing result was not detected earlier.

We find that the values of θ_v is generally lower at cycle maxima and higher at solar minima. Moreover, there is a time lag between the peaks of activity and the dip in latitude. Note that the change in θ_v is also affected by the secondary maximum phases — the two peaks at Cycle 23 maximum appear as two dips; the same is seen for Cycle 24 maximum, though less clearly. If we assume that the solar activity levels affect the tachocline, then a cross-correlation analysis indicates that the dips in θ_v lag the peaks in activity by a little more than three years.

What is also worth noting is that there are cycle-to-cycle variances; the position of the dip in θ_v corresponding to Cycle 23 maximum occurs well after the maximum, but the time lag after Cycle 24 maximum is much smaller. The situation for the Cycle 25 maximum is still unclear, although if one looks at the lag between the times of the first peak in activity and the first dip, one could speculate that Cycle 25 may show a similar time lag as Cycle 23. Here again, we need a few more years of observations to confirm this.

To summarize, we find that the jump of the rotation rate across the tachocline, $\delta\Omega$, changes considerably with time, but the change is not a simple function of solar activity. The jump shows a hysteresis like behavior with respect to the 10.7 cm radio flux, with Cycles 23 and 24 following different patterns while Cycle 25 appears to be mimicking Cycle 24. We also find that the latitude at which $\delta\Omega$ vanishes, i.e., θ_v , shows a significant periodic behavior, being higher at solar minimum and lower at maximum; however, there is a time lag of about 3 years between the minimum of activity and the maximum of θ_v .

3.2. The width, w_d , of the tachocline

Data obtained with 144-day time series are too noisy to determine the time variations of the position, i.e., the midpoint of the tachocline, or the time dependence of the width of the tachocline; consequently, we only show results obtained with data from 720-day time series.

The variation of the width of the tachocline with time is shown in Fig. 6. One can see from that figure that the time dependence at all latitudes is more or less the same, but that the width is larger at the higher latitudes. The latter is a well-known result (H. M. Antia et al. 1998; P. Charbonneau et al. 1999; H. M. Antia & S. Basu 2011), and hence, not surprising.

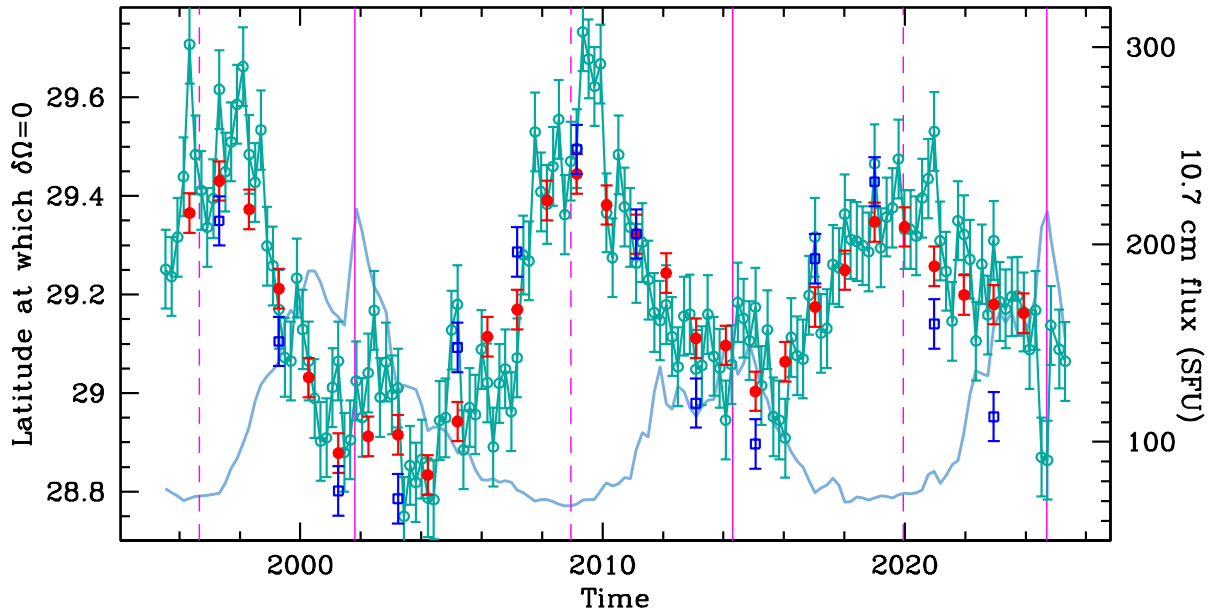


Figure 5. The latitude at which $\delta\Omega = 0$, i.e., θ_v plotted as a function of time. Greenish-blue points are results for 144-day data sets using the SGK pipeline, red points are for 720-day data sets using the SGK pipeline, and blue points are for the 720-day data sets obtained with the GONG project pipeline. The background light blue line shows the 10.7 cm radio flux averaged over 144 days; the magnitude of the radio flux can be read from the axes on the right-hand side of the panel. The solid and dashed vertical lines are epochs of solar maxima and minima, respectively.

While the uncertainties in the measured width at each epoch are large, the variation with time is so smooth that it is conceivable that we have overestimated these uncertainties. It should be noted that the width of the tachocline is the parameter that is the most difficult to determine precisely.

We found that the derived estimates of the width depend heavily on the data uncertainties. Fitting data with low error bars results in smaller width estimates; when using data obtained with much longer time series, namely 2304-day and 4608-day sets, the resulting value of the width is quite small (see *S. Basu & S. G. Korzenik 2025*).

Since all the data sets used in this work have comparable error bars, the resulting time variation cannot be attributed to their variations. Hence, while the value of the width is likely overestimated, the observed time variation is most likely real.

We carried out a number of statistical tests to examine whether the results for the five latitudes shown in Fig. 6 exhibit significant changes over time. We carried out these tests using only the results obtained with SGK data and only for independent sets (i.e., the non-overlapping sets). The first was a simple χ^2 test on the residuals resulting from subtracting the mean width at each latitude from the results of that latitude. As expected, this test indicated that the variations were not statistically significant. The next test was a Durbin-

Watson test (*J. Durbin & G. S. Watson 1971*) on the residuals resulting from performing a linear regression of the data. We first applied it to the time series of the 10.7 cm radio flux, after averaging it over the 720 days corresponding to the SGK data sets to establish a reference since it is known that the 10.7 cm flux changes with time in a quasi-periodic fashion. The test indicated that changes are significant at the 95% confidence level. Results of this test on the width variations however, were inconclusive, with the statistic at each latitude lying between the upper and lower confidence limits for a 95% significance level. The third and final test, a Ljung-Box test (*G. M. Ljung & G. E. P. Box 1978*) gave us results that are more interesting. The 10.7 cm radio flux shows significant autocorrelation at time-lags larger than 2. At latitudes below 45° , the widths show the same behavior as the 10.7 cm flux, but at higher latitudes, the changes are not significant at the largest lags (11 and above). Therefore, although the uncertainties are large, the tests give us evidence that there is a significant periodic time variation in the tachocline width. A cross-correlation of the 10.7 cm flux and the width at each latitude shows that changes in the 10.7 cm occur about four years before changes in w_d , which is why the maximum in w_d appears close to the minimum in the 10.7 cm flux.

To summarize, despite the uncertainties, we find evidence that the width of the tachocline changes in a periodic manner and that the width is larger when activity is

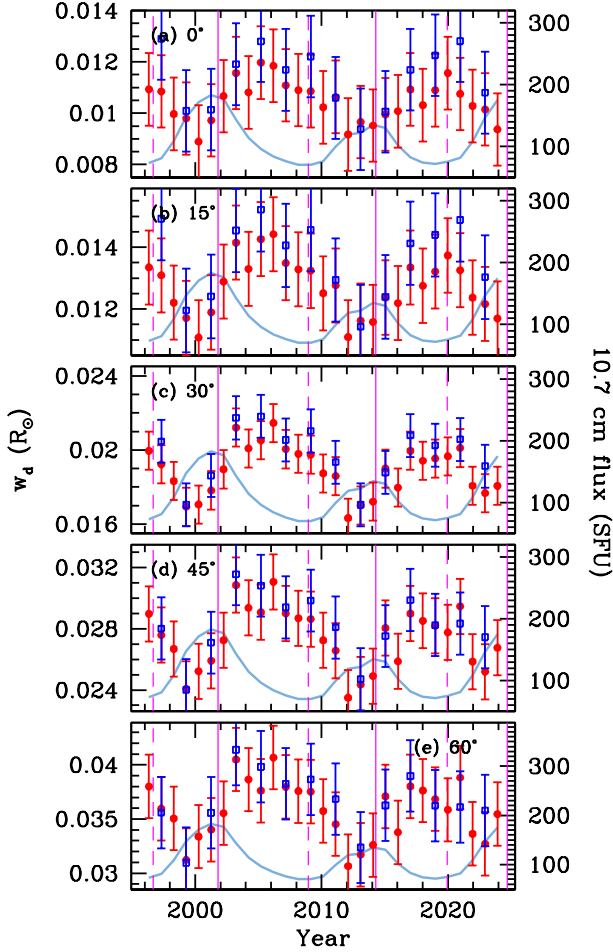


Figure 6. Changes in the width of the tachocline at different latitudes plotted as a function of time. Panels (a)–(e) show the results at latitudes 0, 15, 30, 45, and 60°. Only 720-day results are shown. The red circles are results when using data from the SGK pipeline, and the blue squares are results when using data from the GONG project pipeline. The light blue line shows the 10.7 cm radio flux averaged over 720 days corresponding to the SGK data. The magnitude of the radio flux can be read from the axes on the right-hand side of the panel. The solid and dashed vertical lines are epochs of solar maxima and minima, respectively.

smaller. There is a time lag of about four years between the changes in the activity and changes in the width.

3.3. The position, r_d , of the tachocline

The change in the position of the tachocline is presented in Fig. 7 and shows a more random variation, though again the uncertainties are large; hence, the changes with solar cycle are only marginally statistically significant.

Despite the large uncertainties, we find that at low latitudes, the changes are in lockstep with activity levels during Cycle 23 with r_d increasing with increasing

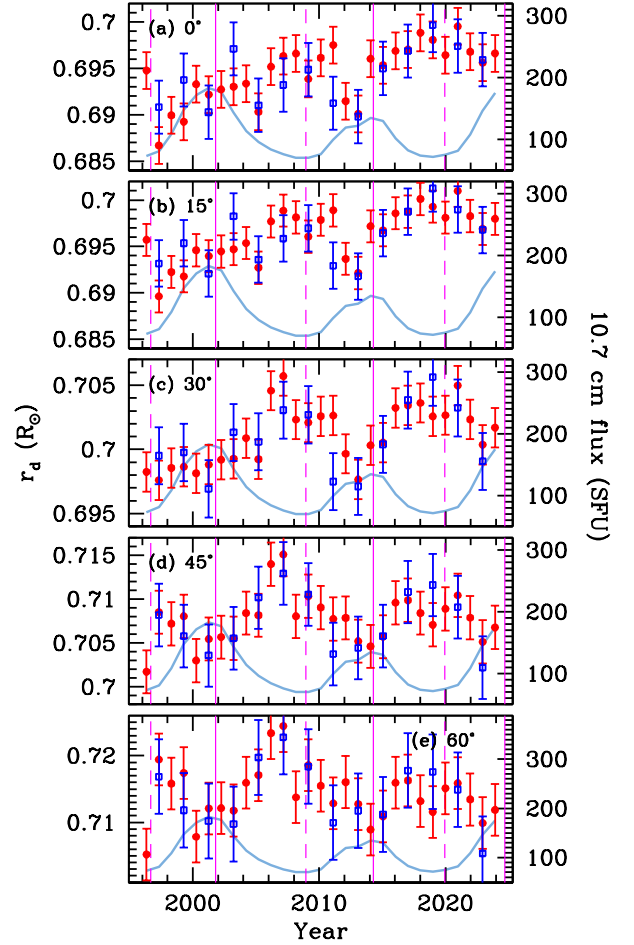


Figure 7. Changes in the position of the tachocline at different latitudes plotted as a function of time. Panels (a)–(e) show the results at latitudes 0, 15, 30, 45, and 60°. Only 720-day results are shown. The red circles are results when using data from the SGK pipeline, and the blue squares are results when using data from the GONG project pipeline. The light blue line shows the 10.7 cm radio flux averaged over 720 days corresponding to the SGK data. The magnitude of the radio flux can be read from the axes on the right-hand side of the panel. The solid and dashed vertical lines are epochs of solar maxima and minima, respectively.

activity, but there appears to be an anti-correlation between position and activity at higher latitudes. The changeover appears to be around a latitude of 30°; around this latitude, the tachocline position was essentially unchanged during Cycle 23. By contrast, for Cycles 24 and 25, the position of the tachocline seems anti-correlated with activity levels, with r_d increasing as activity decreases. There is a hysteresis-like behavior in the position as well; and just as in the case of the jump, variations over Cycle 25 follow those of Cycle 24, but the large uncertainties make this trend less obvious.

The more interesting variation of the position of the tachocline is the secular change at low latitudes, as shown in Fig. 8, while the variation at high latitudes is not statistically significant. As shown in the figure, the tachocline has been moving closer to the base of the convection zone. This secular change can be fitted with a straight line, and the resulting dependence of this slope with latitude is shown in Fig. 9, indicating that it changes sign around a latitude of $49^\circ \pm 15^\circ$.

As in the case of the width, we applied several statistical tests to examine the significance of the time-variation of r_d at the five latitudes shown in Fig 7. Unlike the case of the width, a χ^2 test on the position show a significant change at the equator, 15° and 30° latitudes; the change at 45° is at a 1σ level, while at 60° the changes are not significant. The Durbin-Watson test shows that there is no significant autocorrelation in the results, except at 30° , where the results are inconclusive. Thus the significant change indicated by the χ^2 tests are a result of the secular change in the position. The Ljung-Box test indicates no significant autocorrelation at the equator or at 60° , the results at other latitudes are mixed; results at 15° and 30° show significant autocorrelation (at better than 95% confidence levels) at lags of 2–4 years, and also for lags greater than 22 years, while at 45° , the autocorrelations are significant for lags of 6 to 10 years. Cross correlation between the 10.7 cm radio flux and the tachocline position is significant only at 45° and 60° , with a lag of 4 years. Thus, the periodicity in r_d is less significant than that in the tachocline width.

In summary, we find that the position of the tachocline r_d changes with time are significant. The most interesting behavior is, however, the secular change of r_d , namely that the tachocline has moved closer to the convection-zone base over the last 30 years for which we have high quality helioseismic observations. Although we see a hint of periodic behavior that is anticorrelated with solar activity, it is statistically significant only at the higher latitudes.

4. DISCUSSIONS AND CONCLUSIONS

We have examined how the three parameters we use to characterize the tachocline — i.e., change in rotation rate $\delta\Omega$, or the jump, the position of the midpoint of the tachocline, r_d , and the width of the tachocline, w_d — change as a function of time at different latitudes using 30 years of helioseismic observations acquired by the GONG network. Earlier work on temporal variation of the tachocline used helioseismic data obtained with 72-day or 108-day time series, but the resulting uncertainties did not enable the detection of time variations in the width and position of the tachocline. To circum-

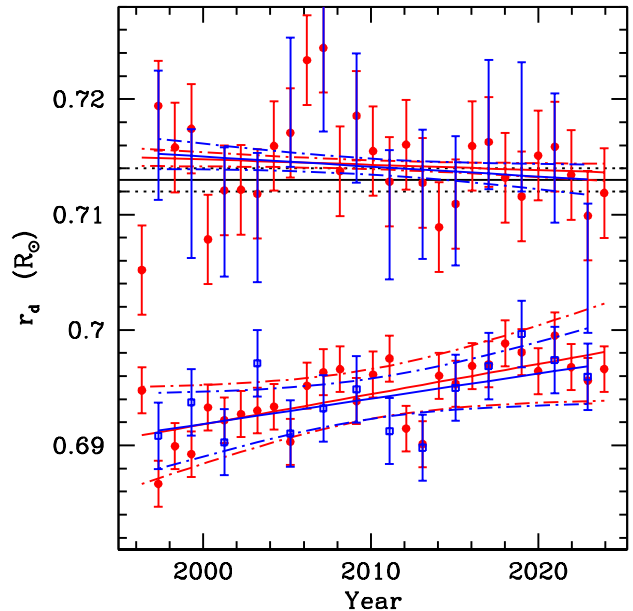


Figure 8. The position of the tachocline at the equator (lower set of points) and at 60° latitude (upper set of points) plotted as a function of time. The red points are results with SGK pipeline data, and the blue points are from the GONG project pipeline. The solid lines of the corresponding colors show the linear least-squares fit to the points, with the dot-dashed lines indicating the 95% significance level. The solid black line marks the position of the convection-zone base, with dotted lines showing the 1σ uncertainty.

vent this, we have used data from longer time series. The jump across the tachocline was determined using rotational splittings obtained with 144-day time series, while the other parameters were obtained with 720-day time series.

The most statistically significant variation with time is that of the jump. The variation is different at different latitudes, and does not show a simple correlation with the level of solar activity. In fact, when plotted as a function of the 10.7 cm radio flux, Cycles 23 and 24 follow different patterns. The rising and falling phases of each cycle, except for the rising phase of Cycle 24, follow a significant linear trend with the 10.7 cm radio flux. Although Cycle 25 is much stronger than Cycle 24, the tachocline jump follows the pattern seen during Cycle 24. This leads us to speculate again (see [S. Basu et al. 2024](#)) that the jump across the tachocline during Cycle 26 will follow the pattern seen during Cycle 23, or in other words, there is a four-solar cycle (i.e., a two Hale-cycle) period in the jump across the tachocline. Of course, we need about 10 more years of helioseismic data to verify our hypothesis. It should be noted that double-Hale cycle variations in the Sun have been re-

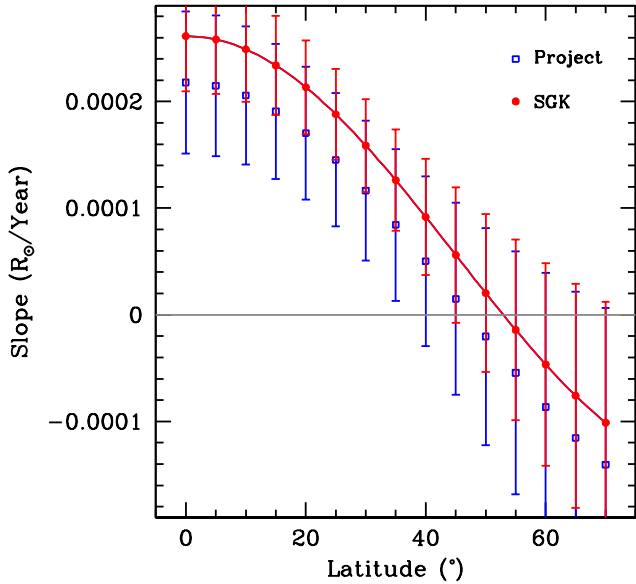


Figure 9. The slope of the temporal variation in the position of the tachocline plotted as a function of latitude. The red points are results obtained with the SGK pipeline 720-day data, the blue points are obtained with the GONG project’s pipeline. For reference, a horizontal line is shown at zero slope.

ported previously. [V. M. Efimenko & V. G. Lozitsky \(2018\)](#) report a two Hale-cycle period in the power-law index for distributions of equivalent diameters of large groups of sunspots (i.e., sizes of 50–90 Mm.) Earlier, [J. Javaraiah \(2003\)](#) reported that the equatorial rotation rate of the Sun shows evidence of a double-Hale cycle.

The latitude at which the jump across the tachocline vanishes, i.e., θ_v , the location that divides the tachocline into a “low- θ ” branch where the convection zone rotates faster than the deep interior and a “high- θ ” branch where the convection zone rotates slower than the deep interior, changes with time. This θ_v latitude is lower at solar maximum, leading us to speculate that such “sloshing” of the tachocline might be related to the magnetic field in the mid-latitude bands. There is currently no scenario that can explain this behavior. The solar convection zone rotation rate and the tachocline have been modeled by [S. A. Balbus \(2009a\)](#) and [S. A. Balbus \(2009b\)](#), who used the thermal wind equation to deduce the shape of the isorotation surfaces in the bulk of the convection zone and the tachocline. This work was extended further by [S. A. Balbus & H. N. Latter \(2010\)](#), who showed that the co-latitude at which the tachocline bifurcated (i.e., where $\delta\Omega = 0$, hence at θ_v) depended on a parameter that depends on the torque exerted by the tachocline on the interior, in particular at the value at which the viscous torque vanishes. Thus, we may

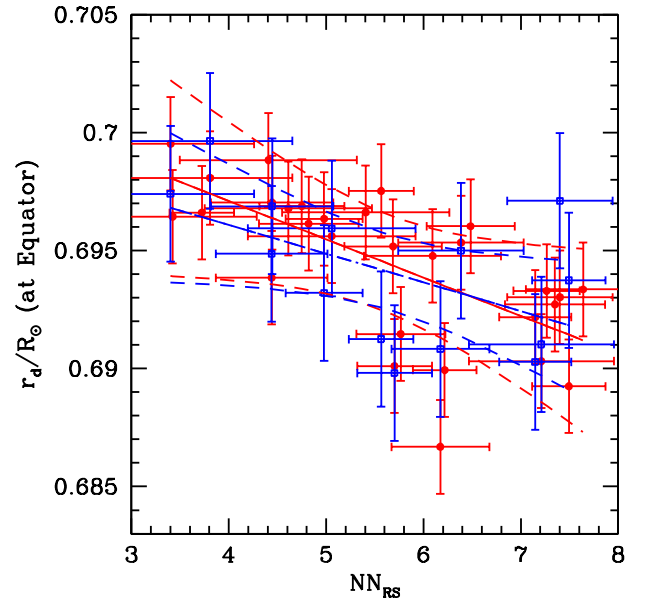


Figure 10. The position, r_d , of the tachocline at the equator plotted as a function of the annual number of sunspots in a sunspot group. The red circles correspond to SGK data, while the blue squares correspond to GONG pipeline data. The solid lines show the corresponding linear fit, while the dashed lines show 95% confidence limits. Sunspot data are from [A. A. Pevtsov et al. \(2025\)](#) courtesy of Alexei Pevtsov.

be tempted to say that the changing θ_v is caused by changing values of the torque; however, as the authors themselves warn, the calculations were done under ideal conditions. Besides, any explanation for the change in θ_v should also explain the lag between θ_v and magnetic activity.

The time variation of the width of the tachocline is not statistically significant if one relies on simple χ^2 statistics. Other statistical tests reveal the presence of periodicities in the data and a significant cross-correlation signal between the width and the 10.7 cm radio flux. If we ignore the large uncertainties, the variation we see suggests the presence of a thinner tachocline when the Sun is most active. This agrees with the predictions of [L. I. Matilsky et al. \(2025\)](#) who found that Maxwell stresses arising from a dynamo-generated non-axisymmetric poloidal field can keep the tachocline from spreading.

Our results on the position of the tachocline, r_d , are somewhat more surprising. Although solar-cycle-related variations are only marginally statistically significant, it does appear that at low activity levels, the position of the tachocline shifts to a higher location. What is surprising, though, is the secular change in r_d , where, at low latitudes, it has been moving to higher radii, and

coming closer to the base of the convection zone. The question that arises naturally, is whether this is an indication of a weakening of the Sun's magnetic field, or some property of the magnetic field, over the last few decades. We believe that there could be a connection with the nature of the solar magnetic field changing over time. Y. A. Nagovitsyn et al. (2012) found a negative correlation between the numbers of small and large sunspots during the period of 1998–2011; the number of large sunspots gradually decreased, while the number of small sunspots steadily increased, indicating a shift in the properties of the solar magnetic field. A. A. Pevtsov et al. (2025) found that the annual number of sunspots in a sunspot group shows a steady decline after one removed the solar cycle variation) since about 1990; the authors believe that the number of sunspots per group may represent active region complexity. As it happens, the position of the tachocline seems to be correlated with the average number of sunspots in sunspot groups. We can see this in Fig. 10 where we plot r_d at the equator as a function of the average number of sunspots per sunspot group. The relation can be fit with a straight line, and the correlation is statistically significant.

To conclude, the solar tachocline changes with time. However, the changes are not a simple function of the solar cycle. There is an indication of a longer period in the variation of the amplitude of the jump across the tachocline, and there has been a secular change in the position of the tachocline for the period over which data are available. The solar-cycle-related changes of

the width and position are barely detectable, even when using data sets obtained with time series that are almost two years long. A more accurate determination of these changes might need other observational approaches and also a better analytical model of the tachocline.

ACKNOWLEDGMENTS

We thank Alexei Pevtsov for providing us with the data on the average number of sunspots in spot groups. We thank the referee for constructive suggestions; we also thank the ApJ statistics editors for suggesting that we perform specific statistical tests. This work is supported by NASA grant 80NSSC23K0563 to SB and NASA grants 80NSSC22K0516 and NNH18ZDA001N-DRIVE to SGK. This work utilizes GONG data obtained by the NSO Integrated Synoptic Program, managed by the National Solar Observatory, which is operated by the Association of Universities for Research in Astronomy (AURA), Inc., under a cooperative agreement with the National Science Foundation and with contribution from the National Oceanic and Atmospheric Administration (NOAA). The GONG network of instruments is hosted by the Big Bear Solar Observatory, High Altitude Observatory, Learmonth Solar Observatory, Udaipur Solar Observatory, Instituto de Astrofísica de Canarias, and Cerro Tololo Interamerican Observatory.

Facilities: GONG, Dominion Radio Astrophysical Observatory

REFERENCES

- Antia, H. M., & Basu, S. 2011, ApJL, 735, L45, doi: [10.1088/2041-8205/735/2/L45](https://doi.org/10.1088/2041-8205/735/2/L45)
- Antia, H. M., Basu, S., & Chitre, S. M. 1998, MNRAS, 298, 543, doi: [10.1046/j.1365-8711.1998.01635.x](https://doi.org/10.1046/j.1365-8711.1998.01635.x)
- Balbus, S. A. 2009a, MNRAS, 395, 2056, doi: [10.1111/j.1365-2966.2009.14469.x](https://doi.org/10.1111/j.1365-2966.2009.14469.x)
- Balbus, S. A. 2009b, MNRAS, 395, 2056, doi: [10.1111/j.1365-2966.2009.14469.x](https://doi.org/10.1111/j.1365-2966.2009.14469.x)
- Balbus, S. A., & Latter, H. N. 2010, MNRAS, 407, 2565, doi: [10.1111/j.1365-2966.2010.17086.x](https://doi.org/10.1111/j.1365-2966.2010.17086.x)
- Basu, S. 1997, MNRAS, 288, 572, doi: [10.1093/mnras/288.3.572](https://doi.org/10.1093/mnras/288.3.572)
- Basu, S., Andrade de Aguiar, W. A. M., & Korzennik, S. G. 2024, ApJ, 975, 276, doi: [10.3847/1538-4357/ad82e6](https://doi.org/10.3847/1538-4357/ad82e6)
- Basu, S., & Antia, H. M. 2019, ApJ, 883, 93, doi: [10.3847/1538-4357/ab3b57](https://doi.org/10.3847/1538-4357/ab3b57)
- Basu, S., & Korzennik, S. G. 2025, arXiv e-prints, arXiv:2511.07534. <https://arxiv.org/abs/2511.07534>
- Charbonneau, P., Christensen-Dalsgaard, J., Henning, R., et al. 1999, ApJ, 527, 445, doi: [10.1086/308050](https://doi.org/10.1086/308050)
- Chatterjee, P., Nandy, D., & Choudhuri, A. R. 2004, A&A, 427, 1019, doi: [10.1051/0004-6361:20041199](https://doi.org/10.1051/0004-6361:20041199)
- Dikpati, M., & Charbonneau, P. 1999, ApJ, 518, 508, doi: [10.1086/307269](https://doi.org/10.1086/307269)
- Durbin, J., & Watson, G. S. 1971, Biometrika, 58, 1. <http://www.jstor.org/stable/2334313>
- Efimenko, V. M., & Lozitsky, V. G. 2018, Geomagnetism and Aeronomy, 58, 1057, doi: [10.1134/S0016793218080066](https://doi.org/10.1134/S0016793218080066)
- Guerrero, G., & de Gouveia Dal Pino, E. M. 2008, A&A, 485, 267, doi: [10.1051/0004-6361:200809351](https://doi.org/10.1051/0004-6361:200809351)
- Hill, F., Stark, P. B., Stebbins, R. T., et al. 1996, Science, 272, 1292, doi: [10.1126/science.272.5266.1292](https://doi.org/10.1126/science.272.5266.1292)
- Javaraiah, J. 2003, A&A, 401, L9, doi: [10.1051/0004-6361:20030272](https://doi.org/10.1051/0004-6361:20030272)

- Korzennik, S. G. 2004, in ESA Special Publication, Vol. 559, SOHO 14 Helio- and Asteroseismology: Towards a Golden Future, ed. D. Danesy, 524.
<https://arxiv.org/abs/astro-ph/0406470>
- Korzennik, S. G. 2008a, *Astronomische Nachrichten*, 329, 453, doi: [10.1002/asna.200710979](https://doi.org/10.1002/asna.200710979)
- Korzennik, S. G. 2008b, in *Journal of Physics Conference Series*, Vol. 118, *Journal of Physics Conference Series*, 012082, doi: [10.1088/1742-6596/118/1/012082](https://doi.org/10.1088/1742-6596/118/1/012082)
- Korzennik, S. G. 2017, in AAS/Solar Physics Division Meeting, Vol. 48, AAS/Solar Physics Division Abstracts #48, 113.02
- Korzennik, S. G. 2018, in *Catalyzing Solar Connections*, 132
- Korzennik, S. G. 2023, *Frontiers in Astronomy and Space Sciences*, 9, 1031313, doi: [10.3389/fspas.2022.1031313](https://doi.org/10.3389/fspas.2022.1031313)
- Korzennik, S. G., & Eff-Darwich, A. 2013, in *Journal of Physics Conference Series*, Vol. 440, *Journal of Physics Conference Series*, 012015, doi: [10.1088/1742-6596/440/1/012015](https://doi.org/10.1088/1742-6596/440/1/012015)
- Korzennik, S. G., & Eff-Darwich, A. 2026, arXiv e-prints, arXiv:2602.02884. <https://arxiv.org/abs/2602.02884>
- Kosovichev, A. G. 1996, *ApJL*, 469, L61, doi: [10.1086/310253](https://doi.org/10.1086/310253)
- Laarhoven, P. J. M., & Aarts, E. H. L. 1987, *Simulated Annealing: Theory and Applications*, doi: [10.1007/978-94-015-7744-1](https://doi.org/10.1007/978-94-015-7744-1)
- Ljung, G. M., & Box, G. E. P. 1978, *Biometrika*, 65, 297, doi: [10.1093/biomet/65.2.297](https://doi.org/10.1093/biomet/65.2.297)
- Matilsky, L. I., Korre, L., & Brummell, N. H. 2025, *ApJL*, 991, L1, doi: [10.3847/2041-8213/ade3e3](https://doi.org/10.3847/2041-8213/ade3e3)
- Nagovitsyn, Y. A., Pevtsov, A. A., & Livingston, W. C. 2012, *ApJL*, 758, L20, doi: [10.1088/2041-8205/758/1/L20](https://doi.org/10.1088/2041-8205/758/1/L20)
- Pevtsov, A. A., Nagovitsyn, Y. A., & Mursula, K. 2025, *SoPh*, 300, 145, doi: [10.1007/s11207-025-02558-1](https://doi.org/10.1007/s11207-025-02558-1)
- Press, W. H., Teukolsky, S. A., Vetterling, W. T., & Flannery, B. P. 1992, *Numerical recipes in FORTRAN. The art of scientific computing* (Cambridge University Press)
- Ritzwoller, M. H., & Lively, E. M. 1991, *ApJ*, 369, 557, doi: [10.1086/169785](https://doi.org/10.1086/169785)
- Scherrer, P. H., Bogart, R. S., Bush, R. I., et al. 1995, *SoPh*, 162, 129, doi: [10.1007/BF00733429](https://doi.org/10.1007/BF00733429)
- Scherrer, P. H., Schou, J., Bush, R. I., et al. 2012, *SoPh*, 275, 207, doi: [10.1007/s11207-011-9834-2](https://doi.org/10.1007/s11207-011-9834-2)
- Schou, J., Antia, H. M., Basu, S., et al. 1998, *ApJ*, 505, 390, doi: [10.1086/306146](https://doi.org/10.1086/306146)
- Tapping, K. F. 2013, *Space Weather*, 11, 394
- Tapping, K. F., & Morton, D. C. 2013, in *Journal of Physics Conference Series*, Vol. 440, *Journal of Physics Conference Series*, 012039
- Vanderbilt, D., & Louie, S. G. 1984, *Journal of Computational Physics*, 56, 259, doi: [10.1016/0021-9991\(84\)90095-0](https://doi.org/10.1016/0021-9991(84)90095-0)